# The influence of potassium substitution for barium on the structure and property of silver-doped germano-gallate glasses

Théo Guérineau, Alexandre Fargues, Yannick Petit, Evelyne Fargin, Thierry Cardinal

# The influence of potassium substitution for barium on the structure and property of silver-doped germano-gallate glasses

Théo Guérineau[a], Alexandre Fargues[a], Yannick Petit[b], Evelyne Fargin[a], Thierry Cardinal[a]

[a] Institut de Chimie de la Matière Condensée de Bordeaux (ICMCB), CNRS, UMR 5026, Pessac, 33608, France
[b] Centre Lasers Intenses et Applications (CELIA), CNRS, UMR 5107, Talence, 33405, France

## Abstract

The structure and crystallization of silver-doped germano-gallate glasses for substitution of potassium for barium ions have been investigated. By means of Raman spectroscopy, a structural study has been carried out revealing a glass network depolymerization with the formation of non-bridging oxygens likely localized on germanium tetrahedra when the barium concentration increases. These structural modifications do not appear to significatively change the silver ion environments or ionic states, as reported on luminescence and optical transmission spectroscopies. A combined differential scanning calorimetry, X-ray diffraction characterization, scanning electron microscopy and micro-luminescence spectroscopy demonstrate that the barium ions introduction tends to stabilize the silver ions and to influence drastically the devitrification and the crystal growth kinetics. Correlations have been established between ionic conductivity, silver distribution and crystal growth mechanisms.

## Introduction

Near- to mid-infrared window (up to 6 µm) is of great interest for many applications in environment and health or in defense and security. Indeed, vibration modes of many pollutant chemical compounds are detectable in this optical window, while a portion of the atmospheric transmission window is located there (1). To make current technologies functional in this wavelength range, it has been essential to design and develop photonic materials compatible with these optical requirements. Compared to other infrared glass systems such as tellurite, chalcogenide and fluoride glasses, germano-gallate glasses possess enhanced chemical, mechanical and thermal resistances, as demonstrated by the Naval Research Laboratory (2,3). Furthermore, in a global issue driven by technological and economic interests of miniaturization, these enhanced properties have attracted the attention of the scientific community to conduct drawing research on some of the most promising germano-gallate compositions (4–6). For practical applications, the investigation of phase separation-inducing ionic migration and crystallization allows to preserve the vitreous state or monitor the glass ceramics fabrication.

The equimolar potassium germano-gallate glass composition $Ga_{33.3}Ge_{33.3}K_{33.3}$ is of interest since its crystallization gives rise to the formation of stochiometric and noncentrosymmetric crystallized phase $KGaGeO_4$ (7,8). Indeed, the scarce ability of a glass composition to crystallize in a noncentrosymmetric stochiometric phase is a great opportunity to conserve a significative match of the refractive index between both the amorphous and crystallized regions.

Fundamentally, the glass devitrification to form a glass-ceramic can occur according to several types of crystal growth kinetics: crystal nucleation at the glass surface which then grow into the bulk, internal crystal growing in the bulk, etc.(9,10) However, some of these crystal growth mechanisms, such as surface crystallization, are usually detrimental to glass-ceramic in their use in optical-related applications. One way to favor the kinetics of a crystalline phase formation in the bulk employs the introduction of a doping element as a nucleating agent. Several cations and anions can be used as nucleating agent ($Ag^+$,$Cr^{3+}$, rare-earth ions, fluorine) (11–14), but Stookey's study then followed by

Glebov's work have highlighted silver ions as a tremendous nucleating agent for photonic applications (15,16).

Recently, some studies from Skopak *et al.* have explored barium and potassium-containing germano-gallate glass crystallization (8,17). From these studies, the formation of a solid solution mixing $KGaGeO_4$ and $BaGa_2O_4$ crystalline phases on the glass surface have been evidenced. In this paper, a series of barium and potassium-containing germano-gallate glasses doped with a fixed amount of silver ions have been studied. These germano-gallate glasses, with the following composition $99\left[33.3GaO_{\frac{3}{2}} + 33.3GeO_2 + (33.3-x)KO_{\frac{1}{2}} + xBaO\right] + 0.5\,AgO_{1/2}$ with $x$ = 0, 5, 10 and 15 cationic%, have been subjected to density, refractive index, optical transmission, electrical conductivity and Raman structural measurements, as well as, scanning electron microscopy. Crystal growth mechanisms study has been explored by differential scanning calorimetry and X-ray diffraction measurements, as well as scanning electron microscopy. Finally, a luminescence investigation, combining steady state and lifetime spectroscopies, has been carried out to investigate the silver optical response.

## Experimental procedures

### 2.1 Glass preparation

A series of glasses has been elaborated corresponding to the cationic composition in Cat% $99[33.3GaO_{\frac{3}{2}} + 33.3GeO_2 + (33.3-x)KO_{\frac{1}{2}} + xBaO] + 0.5AgO_{1/2}$ (namely, GGBK series) with $x$ = 0, 5, 10 and 15 cationic%. The glasses were synthetized from $Ga_2O_3$ (Strem Chemicals – 99.998 %), $GeO_2$ (Fox Chemicals – 99.999 %), $BaCO_3$ (Sigma-Aldrich ≥ 99 %) and $AgNO_3$ (Alfa Aesar – 99.995 %). Once precursors were weighted, they are introduced in a platinum crucible to be melted between 1350 °C and 1400 °C, depending on the glass composition, for 15 hours. The long melting duration is relatively important since it allows for a homogeneous dispersion of silver ions at the atomic scale. A water quenching is conducted to freeze the mixture without disturbing its homogeneity. After a 4 hour-thermal annealing 30 °C below the glass transition temperature, 1 mm-thick GGBK samples are prepared and optically polished on both parallel faces.

### 2.2 Glass physico-chemical characterizations

The density, $\rho$, was determined by Archimedes method using diethyl phthalate as an immersion liquid at room temperature. The measurement precision is estimated to be ± 0.01 g.cm$^{-3}$. Refractive indices were measured with an Abbe refractometer at 480, 589, 644 and 656 nm with an accuracy of ± 0.002. Raman spectra were recorded in the range of 200 – 1000 cm$^{-1}$ at room temperature with a resolution of 2.5 cm$^{-1}$ using a LABRAM 800-HR Raman spectrometer (Horiba Jobin-Yvon), while excited with a single longitudinal mode laser source at 532 nm and collected with a microscope objective 50× - NA 0.75. Both UV-visible and IR transmission spectra were recorded on a Cary 5000 (Varian) spectrometer from 200 nm to 2500 nm by step of 1 nm and Fourier Transform Infrared (Brucker Equinox 55) from 2.5 µm to 7 µm under 200 scans with a 4 cm$^{-1}$ resolution, respectively.

The luminescence spectra (emission and excitation) were recorded with a SPEX Fluorolog-2 spectrofluorimeter (Horiba Jobin-Yvon) at room temperature on glass powder. The excitation source was a 450 W xenon lamp delivering a continuous excitation from 200 nm to 800 nm. Each spectrum was collected with a step and resolution of 1 nm. A Hamamatsu R298 photomultiplier was used as detector. The single photon counting lifetimes were recorded on an Edinburgh apparatus (M300 Monochromator) with 1024 channels and a maximal peak count of 1000, equipped with a nanoflash lamp and a Hamamatsu R298 photomultiplier as detector.

Differential scanning calorimetry (DSC) measurements were performed on a single 70 mg-glass chunk in platinum crucible using a Netzsch DSC Pegasus 404 F3 from 500 °C and 1100 °C. The glass transition temperature *Tg* was defined as the intersection of the base line with the inflexion tangent of the glass transition domain, the beginning temperature of crystallization *Tx* was defined as the intersection of the base line with inflexion tangent of the crystallization peak and the maximal crystallization temperature *Tp* was defined as the maximal point of the crystallization peak.

A home-made apparatus using a four-points technique of platinum electrodes was used to assess the electrical conductivity of the 1 mm-thick polished glass sample, while being placed in an oven working from 20 °C to 1000 °C. The impedance was measured with a Keithley 487 Picoammeter.

### 2.3 Heat-treated glass characterizations

Scanning electron microscopy in back-scattered electron mode was carried out on a GeminiSEM 300 (15 kV and variable pressure) equipped with a Bruker XFlash 6TI60 for the EDX measurements. X-ray scattering were recorded at room temperature on glass heat-treated sample then on ground powder and collected on a PANalitycal X'pert MPD-PRO Bragg-Brentano θ-θ geometry diffractometer equipped with a secondary monochromator, a 3X15 positions sample changer and an X'celerator detector over an angular range of 2θ = 10-80°. Each acquisition lasted for 34 minutes. The Cu-Kα radiation was generated at 45 KV and 40 mA (lambda = 0.15418 nm).

Micro-luminescence was conducted with a LABRAM 800-HR spectrophotometer (Horiba Jobin-Yvon) and a Cassegrain microscope objective (74×, NA 0.65) using an excitation He-Cd laser at 325 nm (Max.200mW). Micro-luminescence spectra were recorded thanks to a thermoelectric cooled CCD Camera (Synapse Model 354308). The experimental spectra were corrected from the detection arm spectral response by a correction function determined using copper chloride as a reference sample.

## Results

### 3.1 Physical-chemical properties

Table 1 Experimental elemental compositions with transition temperatures and concentrations of silver ions per cubic centimeter of the GGBK glasses

| **Glass label** | **$GaO_{3/2}$ (Cat%)** | **$GeO_2$ (Cat%)** | **BaO (Cat%)** | **$KO_{1/2}$ (Cat%)** | **$AgO_{1/2}$ (Cat%)** | **$Ag^+$ ions per $cm^3$ ($x10^{20}$)** | ***Tg* (±3°C)** |
|---|---|---|---|---|---|---|---|
| | ***Exp. (±0.2)*** | ***Exp. (±0.2)*** | ***Exp. (±0.2)*** | ***Exp. (±0.2)*** | ***Exp. (±0.2)*** | | |
| GGK | 32.0 | 34.7 | 0 | 32.8 | 0.5 | 1.3 | 661 |
| GGB5K | 33.9 | 35.1 | 4.8 | 25.6 | 0.6 | 1.6 | 648 |
| GGB10K | 32.6 | 35.1 | 10.1 | 21.7 | 0.5 | 1.3 | 646 |
| GGB15K | 32.9 | 35.1 | 14.8 | 16.6 | 0.6 | 1.6 | 642 |

Hereafter are reported the glass compositions measured by Electron Probe Micro-Analysis (EPMA) in Table 1. Since this elemental analysis technique can easily affected the real quantity of $Ag^+$ due to its ionic migration under the electronic flux, another elementary study has been carried out using Inductively Coupled Plasma Optical Emission Spectroscopy (ICP-OES) and the same glass compositions have been measured. From the density measurements presented in Figure 1a, the concentration of $Ag^+$ per cubic centimeter has been determined and is relatively similar in the entire glass series. The characteristic glass temperatures such as glass transition *Tg*, beginning *Tx* and maximal *Tp* crystallization temperatures have been determined thanks to DSC measurements on a single glass

bulk of 70 mg. *Tg* values have been reported in Table 1. By substituting potassium by barium ions, a clear decrease of the *Tg* is observed and reaches about 15 °C for 15 cationic% of BaO.

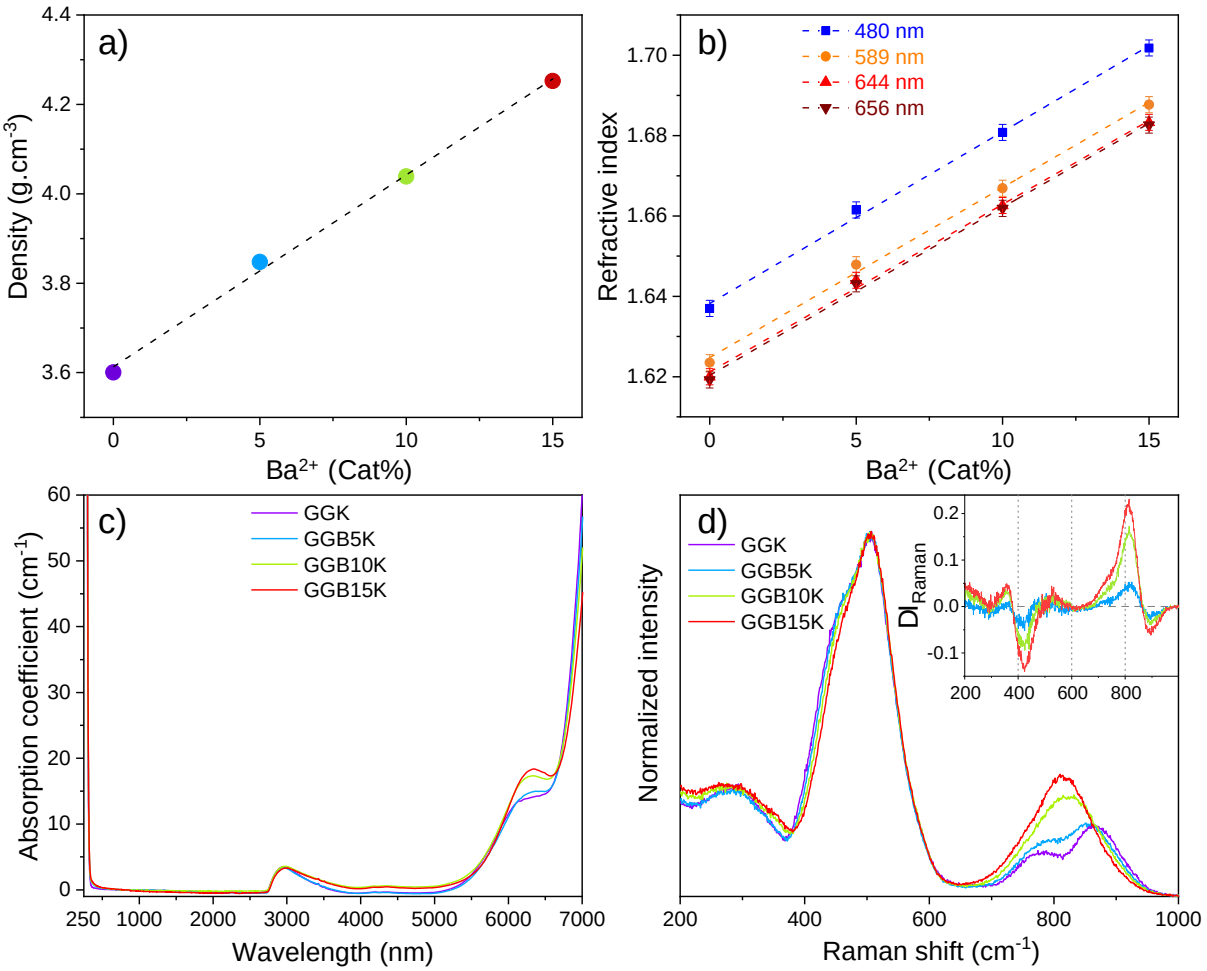


*Figure 1 Properties of the GGBK series as function of the BaO content: (a) Density (b) Refractive indices measured at 480, 589, 644, 656 nm (c) Linear absorption coefficient spectra in UV-Visible-Mid IR region and (d) Raman spectra normalized to the principal band at about 510 cm$^{-1}$ (inset: Raman spectrum difference with GGK glass spectrum). Lines are guides for the eyes for (a) and (b).*

To characterize the impact of potassium ion substitution for barium, glass property analyzes have been performed such as density, refractive index, linear absorption coefficient measurements and Raman spectroscopy. Their evolutions are shown in Figure 1. A linear dependency ($R^2$ = 0.99) of the density from 3.6 g.cm$^{-3}$ at 0 cationic% of $Ba^{2+}$ up to 4.25 g.cm$^{-3}$ at 15 cationic% of $Ba^{2+}$ is observed, suggesting a 0.042±0.002 g.cm$^{-3}$ per cationic%$_{Ba2+}$ (Figure 1a).

In Figure 1b, the refractive index evolution shows an equivalent increase for any measured wavelength (480, 589, 644 and 656 nm), whereas no impact of the substitution could be observed on the refractive index dispersion. As already observed with the density evolution, a linear fit ($R^2$ = 0.99) can be made on the refractive index according to a slope of 0.0042±1E$^{-4}$ per $Ba^{2+}$ cationic percent.

The absorption spectra for linear absorption coefficient up to 60 cm$^{-1}$ are presented on Figure 1c. It shows a strong absorption edge in the UV region from 310 nm ($\lambda_{10\ cm^{-1}}$ = 316 nm) whereas multiphonon absorption edge is located at about 5.5 µm. As no special cares were taken during glass synthesis, OH and $CO_2$ impurities are detected at respectively 3.2 and 4.3 µm. Unlike its silver doped counterparts, GGK glass without silver doping (not shown here) presents a shorter $\lambda_{10\ cm^{-1}}$ cut-off at 270 nm, as reported in the literature (2,17). Thus, the 310 nm-absorption edge is assigned to silver ions in GGBK glasses. In phosphates glasses containing the same silver ions proportion, the presence of a

strong localized absorption edge in the same wavelength domain is in accordance with this assignment (18,19). Lastly, an absorption band peaking at about 6.3 µm increases conjointly to the barium content.

The normalized Raman spectra to the maximum intensity are shown in Figure 1d. Each of them can be decomposed in three parts: low- (200-400 $cm^{-1}$), intermediate- (400-650 $cm^{-1}$) and high-frequency (650-1000 $cm^{-1}$) regions, where the most significant evolutions appear at around 430, 730, 810 and 890 $cm^{-1}$. To better characterize the structural change, spectrum differences ($\Delta I_{Raman}$) are included in the inset. All GGBK glasses present two envelops in the low/intermediate-frequency domain peaking respectively at 300 and 500 $cm^{-1}$. The first one can be assigned to either network-modifying cations vibrating in large interstitial sites (20) or out-of-plane oxygen motions in bent T-O-T bridge (8) (T = Ge or Ga in tetrahedral coordination), while the second one can be attributed to several vibrational contributions of T-O-T bending (20) where the T-O-T oxygen motions are in the bent T-O-T bridge plane (8). A shoulder at 430 $cm^{-1}$ decreases by increasing the barium content, corresponding to an intermediate-frequency region band as highlighted in the differential spectrum. Meanwhile in the high-frequency region of GGK and GGB5K glasses, two bands peak at 780 and 870 $cm^{-1}$ attributed respectively to stretching modes of germanium and gallium tetrahedral units, likely in annular configuration or chain in which the charge on oxygen varies depending on the location of compensating charge cations ($K^+$ or $Ba^{2+}$) (4,8). By increasing the barium content as in GGB10K and GGB15K glasses, a new contribution appears to be predominant lying at 810 $cm^{-1}$, assigned to a symmetric stretching mode of [$GeO_4$] entities containing three bridging oxygens, each links to a T cation, and a non-bridging oxygen engaged in an ionic chemical bond with alkali or alkaline earth ions, denoted [$GeØ_3O^-$] or $Q^3$(20,21). The differential spectrum shows that the appearance of the 810 $cm^{-1}$ band goes hand-in-hand with a new band contribution peaking at 730 $cm^{-1}$ which could be attributed to the antisymmetric stretching mode of the [$GeØ_3O^-$], and the decrease of an un-attributed contribution at around 890 $cm^{-1}$.

The electric conductivity has been measured to evaluate the ionic mobility of the glasses versus the substitution of potassium for barium. In such oxide glass, like in silicate and germanate glasses, the electrical conductivity is predominantly ionic, as described elsewhere (22–25). In GGBK glass family, considering the high concentration of monovalent cations, only $K^+$ and $Ag^+$ are expected to contribute in the overall ionic conductivity (24,26), and accordingly to the relative concentration one can assume that the ionic conductivity if mainly driven by the potassium ions. The ionic conductivity $\sigma$ of containing glasses can be expressed as the following expression (27,28):

$$\sigma = n * \mu * e \quad (1)$$

with $n$ the effective charge carrier concentration, $\mu$ their electrical mobility and $e$ their positive charge.

The activation energy and the ionic conductivity at 25°C has been extracted from the results shown in Figure 2. The barium introduction shifts the measuring region to higher temperature (Figure 2a). In the meantime, the logarithm slope is abruptly increased since the 5 cationic% of BaO introduced and remained fairly constant for larger amount of BaO. Regarding the activation energy ($E_{act}$) on the Figure 2b, $E_{act}$ starts at 0.17 eV (0 cationic% BaO), while more than double to reach 0.37 eV at 5 cationic% of BaO. By increasing the barium content, the $E_{act}$ reaches a maximum at 10 cationic% of barium oxide and slightly decreases for 15 cationic% of BaO. Meanwhile, the conductivity, expressed in Napierian logarithm, seems to follow a general decrease trend from -9.3 $\Omega^{-1}.cm^{-1}$ to -15.6 $\Omega^{-1}.cm^{-1}$. Beyond 10 cationic% of BaO, the electric conductivity remains constant according to the error bars. This evolution is in accordance with the substitution of the single charge potassium ions for the double charged barium ions which contribute to decrease the ionic mobility.

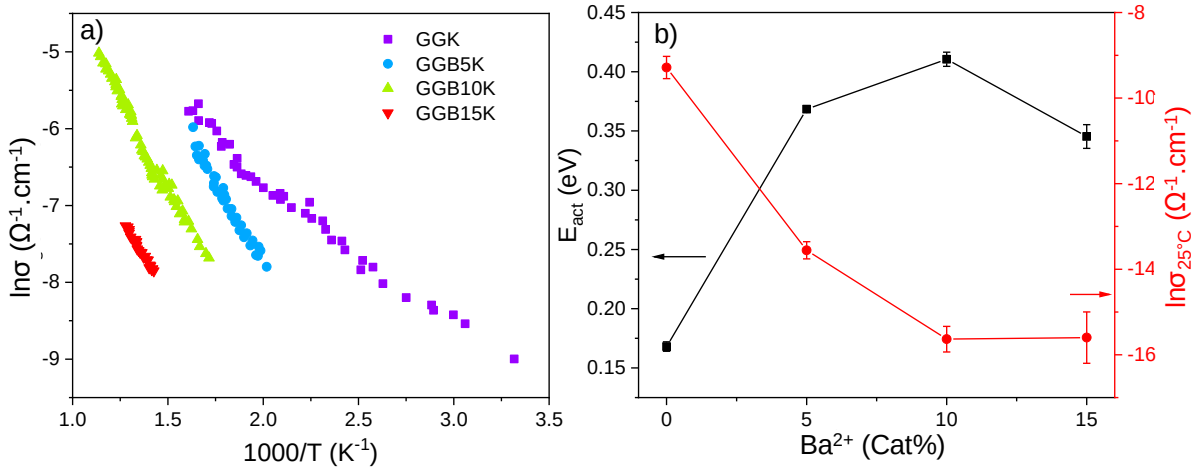


*Figure 2 (a) Napierian log of electrical conductivity measured for GGBK glasses with error bars included in symbol size (b) Determined activation energy (left – black curve) and Napierian log of the conductivity at 25°C (right – red curve) over the barium content.*

The time evolution of the silver-containing glass illustrates the evolution of the ionic mobility versus the substitution of potassium ions for barium ions in the glass composition. The GGK bulk glass after one year exhibits a yellowish coloration (photographs in Figure 3a) attributed to the presence of a new extinction band in the absorption spectrum around 420 nm which can be easily removed by a fine grain surface polishing (2 µm). Similar surface effect can be observed on polished GGK glass after a heat treatment of *Tg+20°C* over 30 min ($GGK_{HT}$). The same heat treatment (*Tg+20 °C* – 30 min) has been carried out on the other GGBK glasses ($GGBK_{HT}$) and the absorption spectra before/after heat treatment are presented in Figure 3b. The difference spectrum between $GGBK_{HT}$ glasses and their untreated counterparts reveals that the extinction tail amplitude in the 300-to-1500 nm wavelength range decreases by increasing the barium content. The tail extinction maximum comes from 4 $cm^{-1}$ at 350 nm for GGB5K up to vanishing at 15 cationic% of BaO. Energy Dispersive X-ray Spectrometry (EDX) has been conducted on the GGB5K glass surface and has revealed the existence of micro-sized region with high concentration of silver.

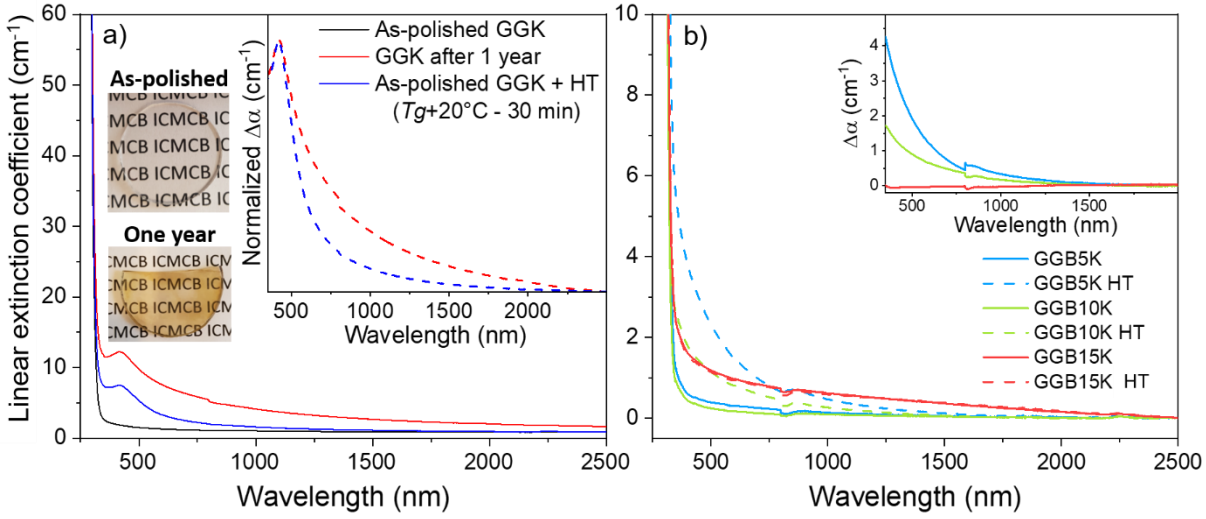


*Figure 3 (a) Linear extinction coefficient of the as-polished GGK glass, after one year and as-polished subjected to heat treatment (HT) of Tg+20 °C over 30 min. Inset: Difference spectra between either the GGK glass after one year or as-polished GGK subjected to HT and the as-polished GGK glass, then normalized at 420 nm (Photographs of the as-polished and after-one-year GGK glasses with a 3 cm-diameter). (b) Linear extinction coefficient of the as-polished $GGB_5K$, $GGB_{10}K$ and $GGB_{15}K$ and their heat-treated counterpart. Inset: Difference spectra for $GGB_5K$, $GGB_{10}K$ and $GGB_{15}K$ between the as-polished and heat-treated glass.*

The luminescence and lifetime (single photon counting) investigations have been performed on silver containing GGBK glasses. The emission spectra for excitation at $\lambda_{exc.}$ = 270, 320 nm and the excitation

spectra for emission at $\lambda_{emi.}$ = 350 and 450 nm are presented hereafter on Figure 4a for the GGK glass. The emission spectrum for excitation at 350 nm reveals large excitation band with a maximum amplitude at 280 nm while the corresponding emission (straight blue line) for excitation around 270 nm highlights a wide emission band centered at around 420 nm. By exciting the glass at 320 nm, a second emission band at 470 nm is observed. The associated excitation spectrum shows an intense band with a maximum at 310 nm. Those luminescence features have been attributed to silver species. Not shown here, the silver-free GGK glass presents a weak emission band peaking at 600 nm ($\lambda_{excitation}$ = 320 nm) with an associated decay time of about 20 µs. This emission is not corresponding to $Ge^{2+}$ center which exhibit UV-excitation and blue-emission bands in germano-silicate glass for instance (29). However, such red luminescence properties observed in silver free sample can be related to the presence of platinum impurity, detected by ICP-OES analysis, which is unintentionally incorporated during the glass synthesis using platinum crucible. Indeed, such microsecond-order red emission has been attributed to $d - d$ platinum transitions of the $Pt^{2+}$ and/or $Pt^{4+}$ ions (30,31).

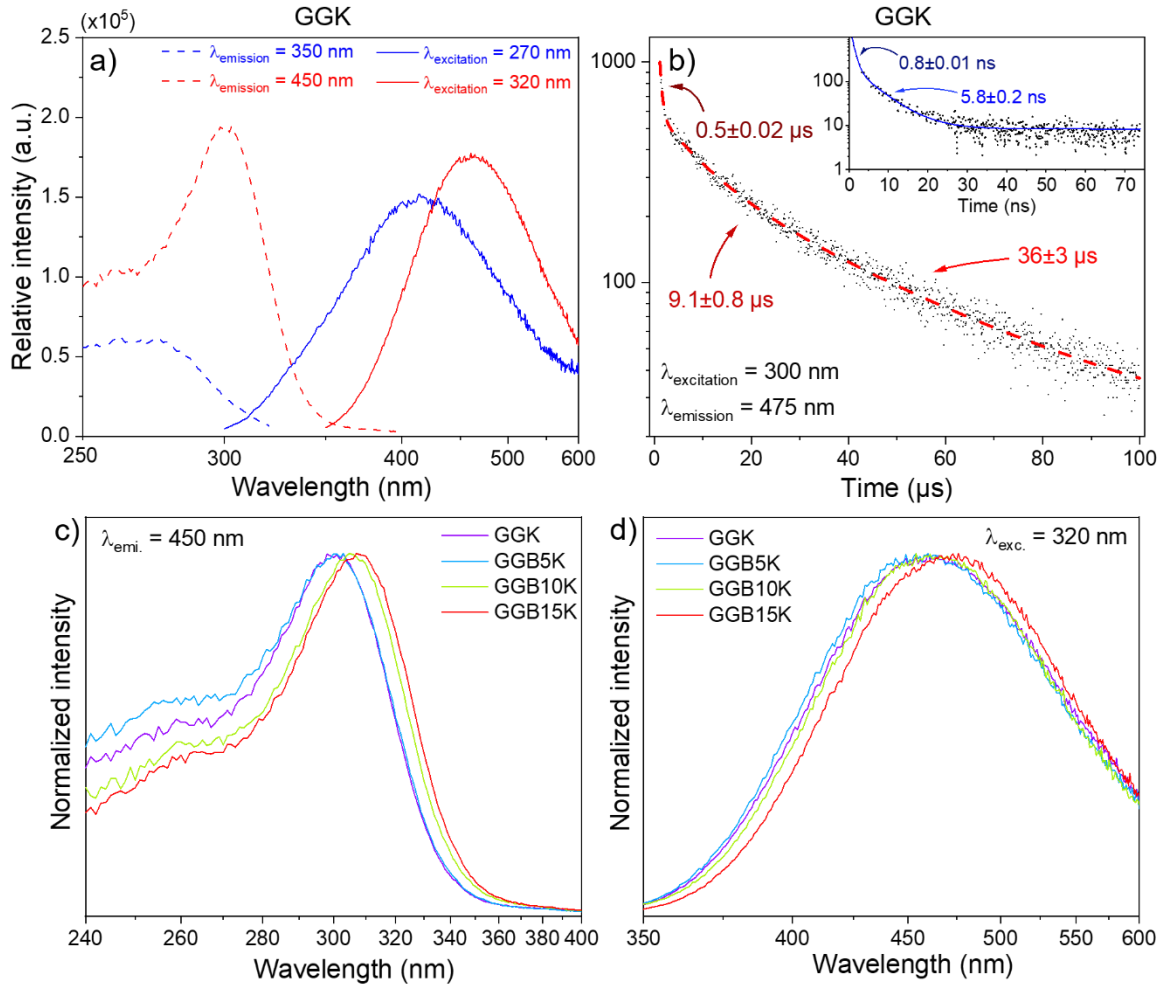


*Figure 4 (a) Excitation and emission spectra of GGK glass; (b) Decay time at micro and nanosecond (inset) time scale for GGK glass; Superposition of GGBK (c) excitation spectra for an emission of 450 nm and (d) emission spectra for an excitation of 320 nm.*

Indeed, the strong luminescence in silver containing glasses is related to the presence of silver species (32,33). The luminescence of silver entities such as isolated ions, pairs and clusters have been widely studied in various glass and in particular in phosphate glass compositions (19,32–36). It has been demonstrated that the luminescence of silver ions and silver cluster can lead to broad emission in the whole visible range for main excitation bands located between 200 nm to 400 nm depending on the silver species. The lifetime measurements allow discriminating those silver emitting centers. Isolated

and aggregated silver ions entities luminescence decay in microseconds order (36), while in nanoseconds order for silver clusters (37).

On Figure 4b are presented the GGK glass decay times at the micro- and nanosecond (inset) temporal scales for an excitation at 300 nm and an emission at 475 nm using a single photon counting system. At the microsecond time scale, a three-exponential decay function could fit the results exhibiting three decay times at 0.5 µs, 9.1 µs and 36 µs. Meanwhile, two shorter decay times are extracted from the nanosecond timescale measurement at 0.8 and 5.8 ns. The shorter nanosecond decay time 0.8 ns is attributed a nanoflash lamp artefact. The existence of those microseconds and nanoseconds lifetimes (Figure 4b) are in accordance with the co-existence of isolated, paired silver ions and silver clusters (33,38). In a meantime, a decay time experiment combining both nano and microsecond timescale have revealed the 5.8 ns decay time associated emission is at least five time more intense than the microsecond decay time's one (not shown here). Thus, a significant quantity of silver clusters seems to be present in the pristine glass.

The normalized emission and excitation spectra for respectively excitation at 320 nm and emission at 450 nm for the GGBK series is reported in Figure 4c and Figure 4d. The spectral distribution is relatively identical and one can observe for both GGB10K and GGB15K glasses, a red shift about 5-20 nm Figure 4 (c,d) as compared to the GGK glass features. The potassium for barium substitution seems not to affect strongly the silver species environment and segregation within the glass matrix.

### 3.3 Crystal growth kinetics

The DSC thermograms for all GGBK glasses have been performed and the crystallization peak regions are presented in Figure 5a in term of cationic value to take into account the difference of molar mass. In all GGBK glasses at least two crystallization peaks can be observed. While substituting the potassium for barium, the crystallization peak amplitude decreases. The *Tx* decreases continuously, while the *Tp* decreases between GGK and GGB5K then increases by adding more barium. To better quantify the evolution, the GGBK glass integrated peak area and crystallization slopes are determined after baseline removal, and then normalized to the maximum. The enthalpy of transition $\Delta H$ can be expressed as the following expression (39,40):

$$\Delta H = C_{cal} * A \quad (2)$$

with $C_{cal}$ the calorimeter constant and $A$ the area under the peak.

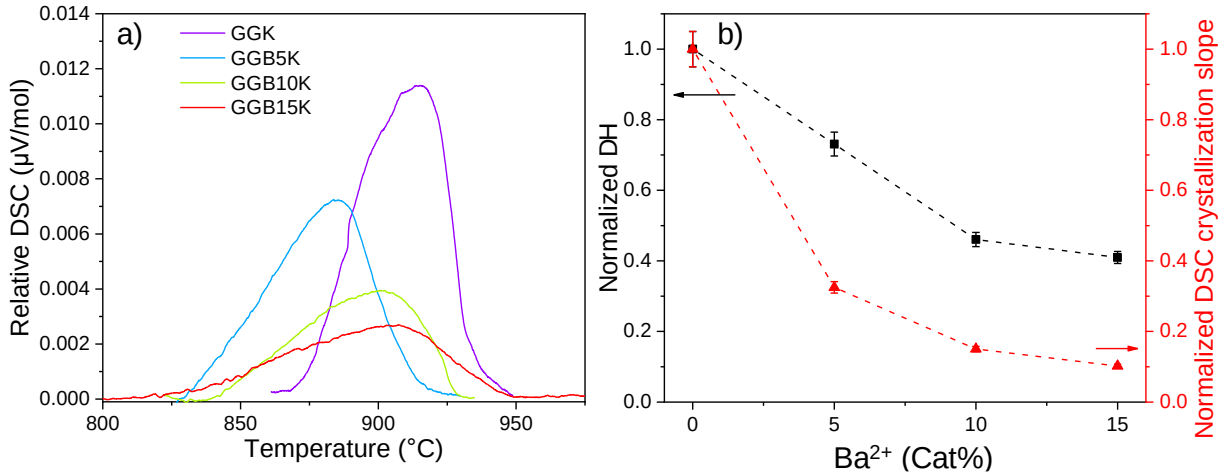


*Figure 5 (a) DSC thermograms after baseline subtraction in the crystallization region (b) Normalized enthalpy of transition deduced from the integrated peak area (left – black curve) and normalized DSC crystallization slope extracted between Tx and Tp (right – red curve) in function of the barium content in GGBK glasses.*

Even though $C_{cal}$ was not measured, the relative $\Delta H$ for each GGBK glasses after normalization can be determined (Figure 5b) since thermograms are recorded on the same apparatus and at constant sample mass (70 mg). Both relative $\Delta H$ and crystallization slope follow approximately the same decrease trend when increasing the barium content.

An air heat treatment at $T_x$-60°C during 5 h on GGBK glasses have been performed on rectangular 1-1.2 mm-thick samples, where the two largest parallel faces were previously optically polished. After the heat treatment, rectangular samples were fractured, then one of the freshly fractured edges was optically polished for all the GGBK glasses.

On Figure 6 are reported the diffractograms of the GGBK glass powders obtained after heat treatment of the GGBK polished bulks at $T_x$-60°C during 5 h. In every sample of the GGBK series, $KGaGeO_4$ phase appears with additional XRD peaks. The presence of these additional peaks highlights the formation of, at least, another crystallized phase. In GGK glass, peaks indexation does not match with any actual known phase, while in GGB5K, GGB10K and GGB15K, the indexation does match with various barium-germano-gallate phases. Indeed, for the GGB5K and GGB15K, only one additional phase is observed with the formula of $BaGa_2Ge_2O_8$ and $Ba_3Ga_2Ge_2O_{14}$, respectively. For GGB10K, these both previous phases are present.

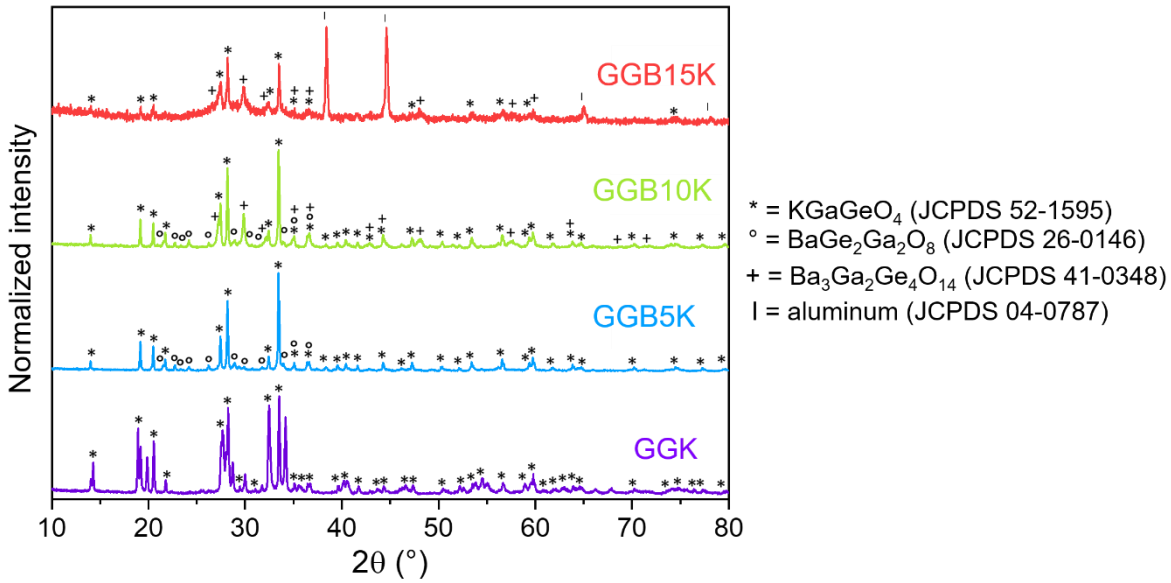


*Figure 6 Diffractograms of GGBK glass powders after heat treatment (Tx-60 °C – 5 h) conducted on bulk then manually ground. * $KGaGeO_4$ phase (JCPDS 52-1595), ° $BaGa_2Ge_2O_8$ phase (JCPDS 26-0146), + $Ba_3Ga_2Ge_2O_{14}$ phase and I aluminum (JCPDS 04-0787).*

After the air heat treatment at $T_x$-60 °C during 5 h of the polished samples, the GGK and GGB10K are no more transparent, whereas GGB5K and GGB15K do. Indeed, in these both latter compositions, the center sample part is transparent, while the glass surface scatter light. A campaign of BSD-SEM characterizations was carried out on the freshly fractured and optically polished edge of GGBK heat-treated samples. The acquisition results are presented in Figure 7 for both GGB5K and GGB15K. In Figure 7(a,b,e,f), the SEM micrographs reveal the formation of dentritic structures with "monolithic form" (≈ 30 µm-thick) and "fractal form" (≈ 5 µm-thick) for GGB5K and GGB15K, respectively. These structures are originating from the glass surface and their locations correspond to the transparency loss area in both glasses. Being perpendicular to the glass surface, the crystalline structures reach a depth of 300 µm in GGB5K and 160 µm in GGB15K. By means of EDX cartographies in both glasses (Figure 7(c,d,g,h)), a high concentration of potassium is reported in the dentritic structures (dark gray region), while barium-rich domains are noticed between these dentritic structures (bright region).

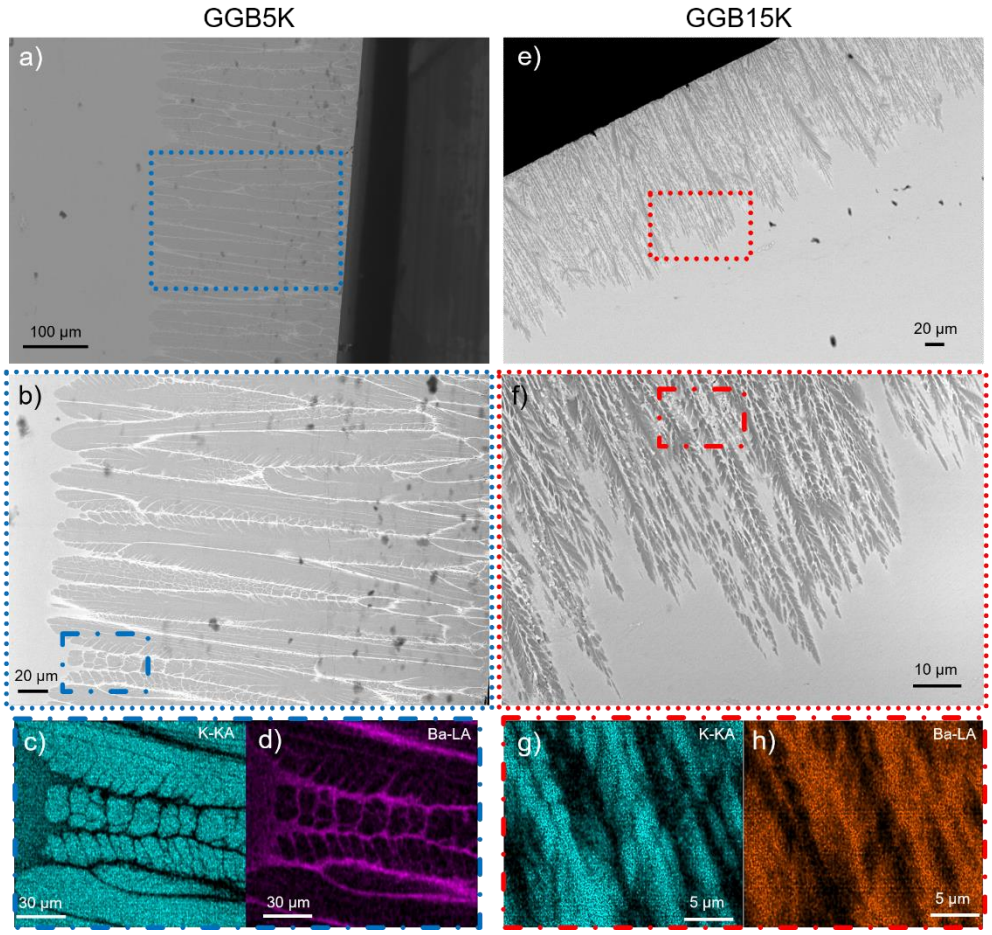


*Figure 7 BSD-SEM micrographs of the freshly fractured and optically polished edge after a heat treatment at Tx-60 °C during 5 h for (a,b) GGB5K and (e,f) GGB15K. EDX cartography for potassium and barium in the crystallized area of both (c,d) GGB5K and (g,h) GGB15K.*

### 3.4 Silver luminescence as a local probe

The silver luminescence spatial distribution have been evaluted after the crystallization induces by heat treatment. The micro-luminescence spectroscopy, using confocal microscope, of the freshly fractured and optically polished edge after a heat treatment at $T_x$*-60 °C* during 5 h has been conducted on both GGB5K and GGB15K for excitation at 325 nm. On Figure 8a and Figure 8c are depicted the spectral feature collected at the dendrite locations (orange curve) and at the center of the samples (blue curve) corresponding to the transparent region. In the GGB5K and GGB15K compositions a wide emission band is observed between 410 nm and 610 nm, however depending on both glass compositions and sample locations the emission maximum is shifting. In both glass compositions the emission maximum in the outer region bands is about 575 nm, while in the inner region emission band maximum is located at 500 nm and 475 nm for GGB5K and GGB15K, respectively. One can notice that the emission spectra in the dendrite location exhibit emission spectra comparable in term of maximum and width to the spectra collected for the pristine samples shown in Figure 4d. In the center location the spectra are red shifted. The emission intensity has been monitored throughout the polished edge for two distinct emission wavelengths, mostly selective to either the inner (425 nm – black dots) or the outer region luminescence (550 nm – red dots) (Figure 8b and Figure 8d). In the GGB5K sample, the fluorescence intensity profile reveals a relatively stable weak intensity in both outer regions (dendrite location) on approximately 300 µm-depth from the glass surface, while in the inner region, a plateau is noticed with a much higher intensity. In the GGB15K sample, the same trend as observed in GGB5K is depicted.

However, for the GGB15K sample, a sharp increase of the intensity is observed at about 160 µm from the glass surface.

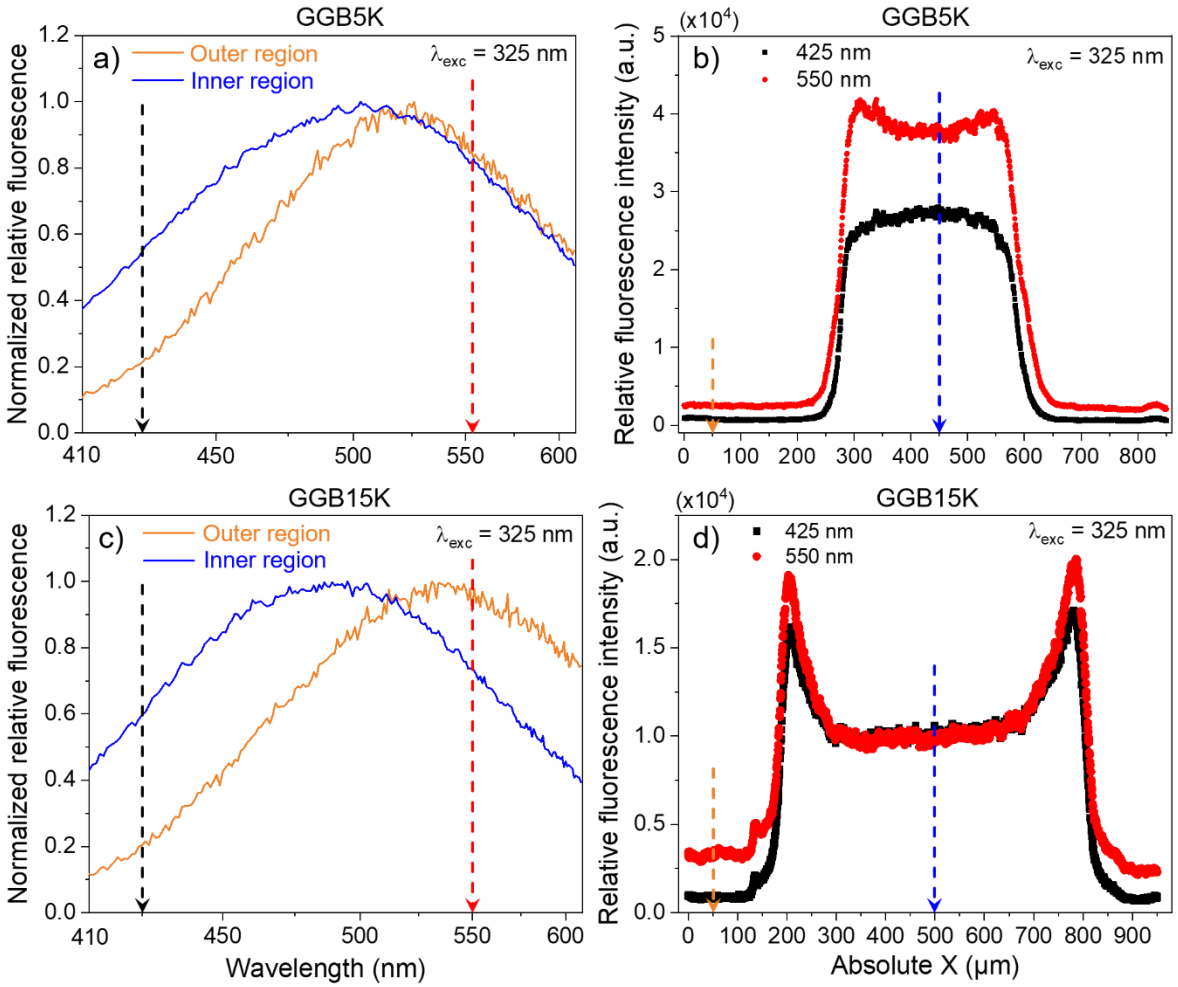


*Figure 8 Micro-luminescence spectroscopy with an excitation at 325 nm of the freshly fractured and optically polished edge after a heat treatment at Tx-60 °C during 5 h. Emission spectra of both (a) GGB5K and (c) GGB15K in the outer and inner regions (red and black doted arrows indicate the selected wavelengths for the intensity profiles in b) and d)). Fluorescence intensity profile extracted from emission spectra at 425 nm and 550 nm of both (b) GGB5K and (d) GGB15K (orange and blue doted arrows indicate the selected positions for the emission bands in a) and c)).*

## Discussion

From the Raman spectroscopy study, various structural changes are clearly visible by substituting the potassium for barium in the GGBK glasses. As previously discussed by Skopak *et al.* in sodium germano-gallate glasses (8), the GGK glass can be described as an assembly of gallium and germanium tetrahedral in which the negative charge of the gallium tetrahedron $[GaO_4]^-$ is compensated by the potassium ions (20,41). While the potassium ions are replaced for barium ions, the antisymmetric and symmetric stretching mode of $[GeØ_3O^-]$ tetrahedra become dominant as compared to the vibration mode assigned to Ge/Ga assemblies in which potassium or barium act as compensating ions. Such variations could be interpreted as originating in the generation of new bonds such as Ge-O-Ba. Indeed, due to the substitution of a monovalent positive ion to a divalent one, this new bond is highly suspected since enough positive charges are now present in the glass network to compensate the negative charge of the $[GaO_4]^-$ tetrahedra. This network evolution hypothesis is in accordance with a modification of the Raman vibration between 400 $cm^{-1}$ and 600 $cm^{-1}$ associated with the decrease of T-O-T bridges.

In view of the structural configuration modifications observed by Raman spectroscopy, the linear evolution of both density and refractive index reports on a continuous structural evolution. One must keep in mind that barium ion has almost twice the molar mass of the heaviest GGK cation, i.e. germanium, and almost twice the polarizability of the most polarizable ion, i.e. potassium. The linear evolution of both density and refractive index with the barium cationic percentage appears directly relate to the substitution of potassium ions for barium ions.

As observed on Figure 2b, the ionic conductivity evolves nonlinearly with the increase of barium content. Such event cannot be explained by a simple variation of charge carrier concentration. The Raman spectroscopy study has evidenced that increasing the barium ions induces both the appearance and the increase of [$GeØ_3O^-$] germanium entities with the presence of non-bridging bonds with a strong ionic bonds character, such as $T - O^- \cdots Ba^{2+}$. Recently we have proposed that the local structure of the GGK glass present similarities with the crystal of the same composition $KGeAlO_4$ exhibiting rings in which the potassium occupy a charge compensation site in channels (42). In the GGK glass one can propose that alkali ions compensate the $[GaO_4]^-$ tetrahedral in rings or chains formed of T-O-T bridges, offering to the potassium ions a strong mobility. When the potassium ions is substituted for the barium ions, the migration path of mobile ions could be progressively obstructed, leading to an electrical conductivity drop (43). The electrical conductivity can be also affected by the formation of [$GeØ_3O^-$] tetrahedra which requires the contribution of more localized positively charge species unlike the relative delocalized negative charge of the gallium tetrahedron $[GaO_4]^-$ of surrounding oxygen. The barium concentration augmentation tends then to increase the energy to promote the $K^+$ ions participation to the electrical conductivity (22,44). One can observe that the effect of barium on the activation energy occurs at low barium concentration and lead to a threshold effect observed between 0 and 5 cationic% of BaO, as shown in Figure 2b. This structural change is proposed also to be at the origin of the drastic improvement of the glass toward ageing and in particular of the silver ions stability.

By means of X-ray diffraction and spectroscopy, as well as BSD scanning electron microscopy, a detailed characterization study has been performed on GGBK glasses after a heat treatment at $T_x$*-60°C* over 5 h. XRD experiments have allowed the identification of the crystallized phases (Figure 6), while X-ray spectroscopy and BSD-SEM have provided the localization of these crystallized phases (Figure 7).

As observed in XRD patterns of all GGBK glasses, the zeolite $KGaGeO_4$ phase provides the most intense and thinner peaks, traducing that this phase is dominant and well crystallized. Meanwhile, in BSD-SEM, the potassium-rich crystallized regions are the most predominant one and correspond to the dendritic motifs. The crystallization of $KGaGeO_4$ phase starts from the glass surface and penetrates in the glass volume. Since the glass and crystal compositions are not stoichiometric for the barium containing glass, the barium ions are pushed progressively leading to a localized region of barium-rich domains, localized between these dendrites (Figure 7(b,c,d) (Figure 7(f,g,h)). The glass experiences a dendrite-like crystallization in the whole volume after the heat treatment in GGK and GGB10K, with probably the presence of remaining amorphous domains between the crystallites. Regarding both GGB5K and GGB15K, the transparent region remaining in the center of the samples is predominantly amorphous according to the Raman response. In all case, the first zeolite crystalline structure $KGeGaO_4$ observed from the glass surface could indicate that the glass network is formed of similar local environment with the association of gallium and germanium ions in tetrahedral sites forming a 3D network in which the alkali ions act as charge compensator. The phase $BaGe_2Ga_2O_8$ appearing for GGB5K on the extremity of $KaGeGaO_4$ crystalline structure is also in line with this hypothesis. As the potassium concentration decreases, a new zeolite phase with barium crystallizes. For GGB10K and GGBK15 corresponding to the highest concentration of barium, the formation of langasite crystallization $Ba_3Ga_2Ge_4O_{14}$ in which the germanium occupy tetrahedral and octahedral sites occurs most probably in the depleted potassium region surrounding the $KGaGeO_4$ phase (45). Thus, the substitution of potassium by barium inhibits the

growth rate of the $KGaGeO_4$, which could likely explain the change of the dendritic forms from "monolithic to "fractal".

The silver ions spatial distribution and the luminescence property are also affected by the crystallization. In the central region of the samples GGB5K and GGB15K out of the crystallization region, the emission spectra of the silver ions shown on Figure 8a and Figure 8c remain similar to the spectra of the glass matrix with a broad emission centered between 450 nm and 500 nm (Figure 4d). Regarding the crystallized area, one can observe for both cases a strong red shift and a narrowing of the emission spectra traducing a change of environment. This phenomenon is combined with a strong decrease of the luminescence intensity. This decrease of the emission intensity is confirmed by the Ag silver element distribution analysis, as shown in Figure 9, which demonstrate for both materials the highest concentration of silver in the uncrystallized glass part than in the dendrite locations.

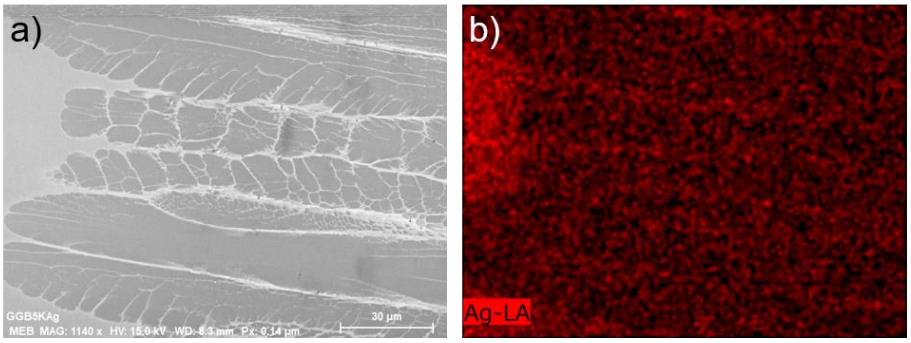


*Figure 9 (a) BSD-SEM micrograph and (b) EDX cartography for silver of the inner-to-outer interface of the GGB5K after a heat treatment at Tx-60 °C during 5 h.*

Determined from the conductivity study (Figure 2), the high conductivity of the GGB5K glass composition is suspected to allow for deepest and fastest migration of silver ion from the outer to the inner glass region rather than in GGB15K with a lowest conductivity. This difference of migration behaviors between these two germano-gallate glasses is observed on the Figure 8b and Figure 8d. Indeed, for the barium-rich glass composition, the appearance of a high intensity increases between the strict inner and outer region, not significantly observed in the barium-poor composition, could be related to a stacking of silver ions or entities in the vicinity of the inner-to-outer interface due to the weak ionic conductivity of this glass. Moreover, the weak luminescence intensity (Figure 8b and Figure 8d) reported on both outer regions of each glass composition (GGB5K and GGB15K) is spatially correlated to the presence of dendrites (Figure 7).

These observations emphasize a lower solubility of the silver ions or species in the dendrites (outer region) than in the amorphous region (inner region). This phenomenon indicates that the silver solubility in the zeolite or the langasite crystalline phases is limited. Considering the spectral distributions of both GGB5K and GGB15K in their dendrites are identical, the remaining species trapped in and/or between dendrites could be highly likely similar.

## Conclusion

Barium and potassium-containing germano-gallate glasses doped with silver ions have been explored to determine the effect of potassium substitution for barium on the glass network and the influence on the crystal growth mechanisms. A linear dependency with barium content of both density and refractive index has been evidenced, while the transmission window has been barely affected. Both potassium and barium are supposed to occupy a charge-compensating site along T-O-T chains or rings formed of $GeO_4$ and $GaO_4$ tetrahedra. The barium introduction affects the ionic mobility and the surface crystallization of zeolite crystalline phase. For large barium concentration, the dendritic crystalline zeolite phase occurring at the early stage starting from the glass surface is giving way to the formation of langasite crystalline phase.

## Acknowledgement

Authors would like to thank Stéphane Relexans for electrical conductivity measurements, Isabelle Svahn for the scanning electron microscopy, Nithavong Cam for the electron probe micro-analysis, Lilian Eloy for the Inductively Coupled Plasma Optical Emission Spectroscopy and Eric Lebraud for the X-ray diffraction characterization. This research was supported by the Agence Nationale de la Recherche (ANR) (ANR-17-CE08-0042-01) and the New Aquitaine Region as well as grants of the Agence Nationale de la Recherche (ANR) with the program “Investissement d’avenir” number ANR-10-IDEX-03-02.

## References


1. Schliesser A, Picqué N, Hänsch TW. Mid-infrared frequency combs. Nature Photonics. juill 2012;6(7):440-9.

2. Bayya SS, Chin GD, Sanghera JS, Aggarwal ID. Germanate glass as a window for high energy laser systems. Optics Express. 2006;14(24):11687.

3. Bayya SS, Harbison BB, Sanghera JS, Aggarwal ID. BaO-Ga2O3-GeO2 glasses with enhanced properties. Journal of Non-Crystalline Solids. 1997;212:198-207.

4. Guérineau T, Strutynski C, Skopak T, Morency S, Hanafi A, Calzavara F, et al. Extended germano-gallate fiber drawing domain: from germanates to gallates optical fibers. Optical Materials Express. 1 juin 2019;9(6):2437.

5. Wen X, Tang G, Yang Q, Chen X, Qian Q, Zhang Q, et al. Highly Tm3+ doped germanate glass and its single mode fiber for 2.0 μm laser. Sci Rep. avr 2016;6(1):20344.

6. Wen X, Tang G, Wang J, Chen X, Qian Q, Yang Z. Tm3+ doped barium gallo-germanate glass single-mode fibers for 2.0 μm laser. Opt Express. 23 mars 2015;23(6):7722.

7. Colbeau-Justin C, Wallez G, Quarton M. Synthesis, crystal growth and crystallographic data of A'GaGe04 compounds (A = K, Rb, Cs, TI). Journal of materials science letters. 1995;14:1260-2.

8. Skopak T, Kroeker S, Levin K, Dussauze M, Méreau R, Ledemi Y, et al. Structure and Properties of Gallium-Rich Sodium Germano-Gallate Glasses. The Journal of Physical Chemistry C. 17 janv 2019;123(2):1370-8.

9. Zanotto ED. Experimental Studies of Surface Nucleation and Crystallization of Glass. Ceramic Transactions, Nucleation and Crystallization in Liquids and Glasses. 1992;30:65-74.

10. Bertrand A, Carreaud J, Delaizir G, Duclère J-R, Colas M, Cornette J, et al. A Comprehensive Study of the Carbon Contamination in Tellurite Glasses and Glass-Ceramics Sintered by Spark Plasma Sintering (SPS). Ballato J, éditeur. Journal of the American Ceramic Society. janv 2014;97(1):163-72.

11. Smogor H, Cardinal T, Jubera V, Fargin E, Videau JJ, Gomez S, et al. Effect of silver on phase separation and crystallization of niobium oxide containing glasses. Journal of Solid State Chemistry. juin 2009;182(6):1351-8.

12. Karamanov A, Pisciella P, Pelino M. The Effect of Cr2O3 as a Nucleating Agent in Iron-rich Glass-ceramics. :5.

13. Garai M. Rare earth ion controlled crystallization of mica glass-ceramics. Journal of Alloys and Compounds. 2016;10.

14. Guo X, Yang H, Cao M. Nucleation and crystallization behavior of Li2O–Al2O3–SiO2 system glass–ceramic containing little fluorine and no-fluorine. Journal of Non-Crystalline Solids. août 2005;351(24-26):2133-7.

15. Stookey SD. Photosensitive Glass. Industrial and engineering chemistry. 1949;41(4):856-61.

16. Efimov OM, Glebov LB, Glebova LN, Richardson KC, Smirnov VI. High-efficiency Bragg gratings in photothermorefractive glass. Applied Optics. 1 févr 1999;38(4):619.

17. Skopak T, Calzavara F, Ledemi Y, Célarié F, Allix M, Véron E, et al. Properties, structure and crystallization study of germano-gallate glasses in the Ga2O3-GeO2-BaO-K2O system. Journal of Non-Crystalline Solids. juin 2019;514:98-107.

18. Bourhis K. Photostructuration par laser infrarouge femtoseconde de verres photosensibles de phosphates de zinc, d'argent et de gallium. 2011.

19. Guérineau T, Loi L, Petit Y, Danto S, Fargues A, Canioni L, et al. Structural influence on the femtosecond laser ability to create fluorescent patterns in silver-containing sodium-gallium phosphate glasses. Optical Materials Express. 1 déc 2018;8(12):3748.

20. McKeown DA, Merzbacher CI. Raman spectroscopic studies of BaO-Ga2O3-GeO2 glasses. Journal of Non-Crystalline Solids. avr 1995;183(1-2):61-72.

21. Skopak T, Hee P, Ledemi Y, Dussauze M, Kroeker S, Cardinal T, et al. Mixture experimental design applied to gallium-rich GaO3/2-GeO2-NaO1/2 glasses. Journal of Non-Crystalline Solids. janv 2017;455:83-9.

22. Anderson OL, Stuart DA. Calculation of Activation Energy of Ionic Conductivity in Silica Glasses by Classical Methods. Journal of the American Ceramic Society. déc 1954;37(12):573-80.

23. Kamitsos EI, Yiannopoulos YD, Jain H, Huang WC. Far-infrared spectra of alkali germanate glasses and correlation with electrical conductivity. Physical Review B. 1 oct 1996;54(14):9775-83.

24. Natrup FV, Bracht H, Murugavel S, Roling B. Cation diffusion and ionic conductivity in soda-lime silicate glasses. Physical Chemistry Chemical Physics. 2005;7(11):2279.

25. Thomas M, Peterson N. Electrical conductivity and tracer diffusion in sodium germanate glasses☆. Solid State Ionics. déc 1984;14(4):297-307.

26. Mehrer H, Imre AW, Tanguep-Nijokep E. Diffusion and ionic conduction in oxide glasses. Journal of Physics: Conference Series. 1 mars 2008;106:012001.

27. Rodrigues ACM, Nascimento MLF, Bragatto CB, Souquet J-L. Charge carrier mobility and concentration as a function of composition in $AgPO_3$–AgI glasses. The Journal of Chemical Physics. 21 déc 2011;135(23):234504.

28. Martin SW. Ionic Conduction in Phosphate Glasses. Journal of the American Ceramic Society. août 1991;74(8):1767-84.

29. Zhao J, Yang Z, Yu C, Qiu J, Song Z. Influence of glass composition on photoluminescence from $Ge^{2+}$ or Ag nano-cluster in germanate glasses for white light-emitting diodes. Journal of the American Ceramic Society. mars 2019;102(3):1169-79.

30. Boiruchon D, Desevedavy F, Chenu S, Strutynski C, Smektala F, Gadret G, et al. Investigation of the Na2O/Ag2O ratio on the synthesis conditions and properties of the 80TeO2–10ZnO–[(10−x)Na2O–xAg2O] glasses. Journal of Non-Crystalline Solids. déc 2019;525:119691.

31. Bevilacqua JM, Eisenberg R. Synthesis and Characterization of Luminescent Square-Planar Platinum(II) Complexes Containing Dithiolate or Dithiocarbamate Ligands. Inorganic Chemistry. juin 1994;33(13):2913-23.

32. Belharouak I, Parent C, Tanguy B, Le Flem G, Couzi M. Silver aggregates in photoluminescent phosphate glasses of the `Ag2O–ZnO–P2O5' system. Journal of Non-Crystalline Solids. mars 1999;244(2-3):238-49.

33. Belharouak I, Parent C, Gravereau P, Chaminade JP, Le Flem G, Moine B. Luminescent Properties of Silver(I) Diphosphate of Compositions Na2−xAgxZnP2O7. Journal of Solid State Chemistry. févr 2000;149(2):284-91.

34. Fares H, Castro T, Orives JR, Franco DF, Nalin M. White light and multicolor emission tuning in Ag nanocluster doped fluorophosphate glasses. RSC Advances. 2017;7(70):44356-65.

35. de Castro T, Fares H, Khalil AA, Laberdesque R, Petit Y, Strutinski C, et al. Femtosecond laser micro-patterning of optical properties and functionalities in novel photosensitive silver-containing fluorophosphate glasses. Journal of Non-Crystalline Solids. août 2019;517:51-6.

36. Petit Y, Danto S, Guérineau T, Abou Khalil A, Le Camus A, Fargin E, et al. On the femtosecond laser-induced photochemistry in silver-containing oxide glasses: mechanisms, related optical and physico-chemical properties, and technological applications. Advanced Optical Technologies. 25 oct 2018;7(5):291-309.

37. Bourhis K, Royon A, Papon G, Bellec M, Petit Y, Canioni L, et al. Formation and thermo-assisted stabilization of luminescent silver clusters in photosensitive glasses. Materials Research Bulletin. avr 2013;48(4):1637-44.

38. Bellec M, Royon A, Bourhis K, Choi J, Bousquet B, Treguer M, et al. 3D Patterning at the Nanoscale of Fluorescent Emitters in Glass. The Journal of Physical Chemistry C. 23 sept 2010;114(37):15584-8.

39. Dean J. Analytical Chemistry Handbook. Mc Graw-Hill. 1995.

40. O'Neill MJ. The Analysis of a Temperature-Controlled Scanning Calorimeter. Analytical Chemistry. juin 1964;36(7):1238-45.

41. Merzbacher CI, McKeown DA. X-ray absorption studies of Ge and Ga environments in BaO-Ga2O3-GeO2 glasses. Journal of Non-Crystalline Solids. 1993;162:81-100.

42. Lampert G, Böhme R. The crystal structure of KAlGeO4. Zeitschrift für Kristallographie. 1986;176:29-33.

43. Terai R, Kitaoka T. The effects of various divalent ions on the migration of sodium ions in the silicate glasses. Journal of the Ceramic Association, Japan. 1968;76:31-7.

44. Amma S, Lanagan MT, Kim SH, Pantano CG. Ionic Conductivity in Sodium-Alkaline Earth-Aluminosilicate Glasses. Dunn B, éditeur. J Am Ceram Soc. avr 2016;99(4):1239-47.

45. Bezmaternykh LN, Vasil'ev AD, Gudim IA, Temerov VL. The growth and structure of Pb3Ga2Ge4O14 and Ba3Ga2Ge4O14 single crystals. Crystallography Reports. mars 2004;49(2):271-4.